scientific reports

Check for updates

OPEN

# Comprehensive investigation of emission homogeneity of InGaAs multiple quantum wells using spatially resolved spectroscopy

Andrea Zelioli[1]✉, Aivaras Špokas[1,2], Bronislovas Čechavičius[1], Martynas Talaikis[1], Sandra Stanionytė[1], Virginijus Bukauskas[1], Augustas Vaitkevičius[1,2], Aurimas Čerškus[1], Piotr Wojnar[3], Vitaly Deibuk[4], Evelina Dudutienė[1] & Renata Butkutė[1,2]✉

**In this study the emission homogeneity of InGaAs multiple quantum wells (MQW) was investigated. Two sets of samples grown by molecular beam epitaxy, with varying In content and QW thickness as well as barrier thickness, were mapped using room temperature photoluminescence and micro-photoluminescence. The result showed that increasing In content leads to a higher stress accumulation which can lead to the formation of a denser net of lattice mismatch dislocations in the QW layer. Samples with optimized barrier design exhibit uniform emission intensity.**

Semiconductor lasers are a class of devices in which the light is generated via stimulated emission in a semiconductor gain media. They are employed in various applications due to the small device size, monochromaticity, high light density, and coherence.

The vertical-cavity surface-emitting laser (VCSEL) is a type of semiconductor laser, in which a gain medium is encapsulated between two distributed Bragg reflectors (DBRs), and light is emitted from the device surface. VCSELs are electrically pumped; because of it the DBRs need to be doped to act as contact layers. The need for contacts on the same surface, from which light is emitted, limits the emission area of the final device, and leads to technological difficulties in the growth.

To overcome this limitation, the vertical-external-cavity surface-emitting-laser (VECSEL) gain chip, in which the upper DBR is substituted by an external coupler, was developed. The external cavity geometry is suitable for optical pumping, and grants access to the laser cavity for the insertion of intracavity elements such as saturable absorber for mode locking[1], nonlinear crystals for frequency doubling[2] or multiple VECSEL chips increasing output power while keeping high beam quality[3–5]. Another more key feature of VECSEL is the output power scalability. VECSELs have been demonstrated with output power from 0.5 W[6] up to 106 W[7] without sacrificing beam quality. This power scalability comes from the possibility of increasing the pump power on the VECSEL chip by increasing the surface that is pumped.

Lasers generating 976 nm light find applications both as a pumping source for erbium doped fiber, and for the generation of 488 nm light via second harmonic generation (SHG)[8]. In the case of 976 nm wavelength VECSEL the maximum output power recorded was 20 mW[9]. The limiting factor was the pumping area; lasing was not observed for areas with diameter greater than 50μm. The demonstrated pumping area is consistent with other published results[10,11].

Different combinations of materials can be used to fabricate the DBR and the multiple quantum wells (MQW). For VECSEL with 976 nm emission, AlAs and GaAs for the DBR growth and InGaAs/GaAs for the MQWs are most often used.

To maximize the output power density of the device it is necessary to suppress In segregation, and avoid the formation of dislocations in the QW structure. In the active area, it is necessary to grow quantum wells with very defined In content and quantum well width to be able to select the correct emission wavelength. It was demonstrated that high substrate temperature during molecular beam epitaxy (MBE) growth has a strong effect

[1]State research institute Center for Physical Sciences and Technology, Saulėtekio al. 3, LT-10257 Vilnius, Lithuania. [2]Institute of Photonics and Nanotechnology, Vilnius University, Saulėtekio al. 3, LT-10257 Vilnius, Lithuania. [3]Institute of Physics, Polish Academy of Sciences, Al. Lotników 32/46, PL-02-668 Warsaw, Poland. [4]Chernivtsi National University, St. Kotsyubyns'koho 2, UA-58012 Chernivtsi, Ukraine. ✉email: andrea.zelioli@ftmc.lt; renata.butkute@ftmc.lt

on In segregation to the surface of the QW layer, this in turn has been shown to affect shape and energy of the photoluminescence (PL) spectrum[12–14].

The main focus of the investigation of InGaAs MQWs in the last five years is on the improvement of quantum confinement using AlGaAs barrier[15,16], micro-characterization of optical properties of nanoscale structures such as nanospades[17] and studies on the improvement of quality structures in low temperature growth conditions and high strain structures[18–20].

Indium segregation can be suppressed via kinetic limitation, either by limiting the As overpressure or by growing the sample at lower substrate temperatures[21]. However, both approaches lead to a lower crystalline quality and weaker PL intensity[12]. The lower growth rate (400 nm/h) has also been shown to lead to sharper interfaces between the QW and barrier layers, enhancing the optical efficiency of the structure[22,23].

In Fitzgerald et al.[24] it was demonstrated that lattice dislocations act as non-radiative recombination centers; they lead to a drop in PL emission intensity and result in the presence of a net of reduced PL intensity. The presence of these non-radiative recombination centers affects the emitters in two main ways: it reduces the overall efficiency of the gain chip, decreasing the output power and leads to the generation of localized heat in the device[25].

To avoid lattice dislocations, strain compensation is usually used. In particular InGaAs/GaAs QWs can be compensated by GaAsP layers placed at the nodes of the optical field of the VECSEL[26,27]. Another possible solution is to use the so called diluted nitrides; this approach consists in alloying low nitrogen content, typically less than 2 %, in the InGaAs QWs, reducing the In content needed to obtain an emission at the same wavelength, with the net effect of reducing the lattice mismatch[28–31]. The main drawback of this method is that the incorporation of nitrogen generally leads to the formation of point defects. Therefore, the use of designs that do not require to employ strain balancing strategies is highly desirable.

This work is focused on optimization of the MBE growth process for application of InGaAs QWs separated by GaAs barriers in VECSEL active area emitting at 976 nm. Both QW thickness and In content were varied to achieve the target emission wavelength. Investigations were performed for large areas using room temperature photoluminescence (RTPL) and micro-photoluminescence (μ-PL), in order to determine the influence of the composition of the QW and the barrier design on the optical quality of the heterostructures.

## Methods

### Growth of InGaAs/GaAs multiple QW

Two types of structure were grown. Both comprised of 12 InGaAs QWs, in Fig. 1(a) the first type of structure, type A, all the QWs are separated by GaAs barriers of 7 nm.

In Fig. 1(b) the second type of structure, type B, is represented. Six pairs of QWs separated by thick barriers. This structure was used to mimic the final VECSEL chip. To maximize the coupling between the laser mode and the QWs, the barrier thickness was calculated for a couple of QW placed at the antinodes of the optical field.

The thickness can be determined by requiring that the sum of the optical thicknesses of the thick barrier, one QW, and half the of the thin barrier, equals half the target wavelength. This condition can be mathematically

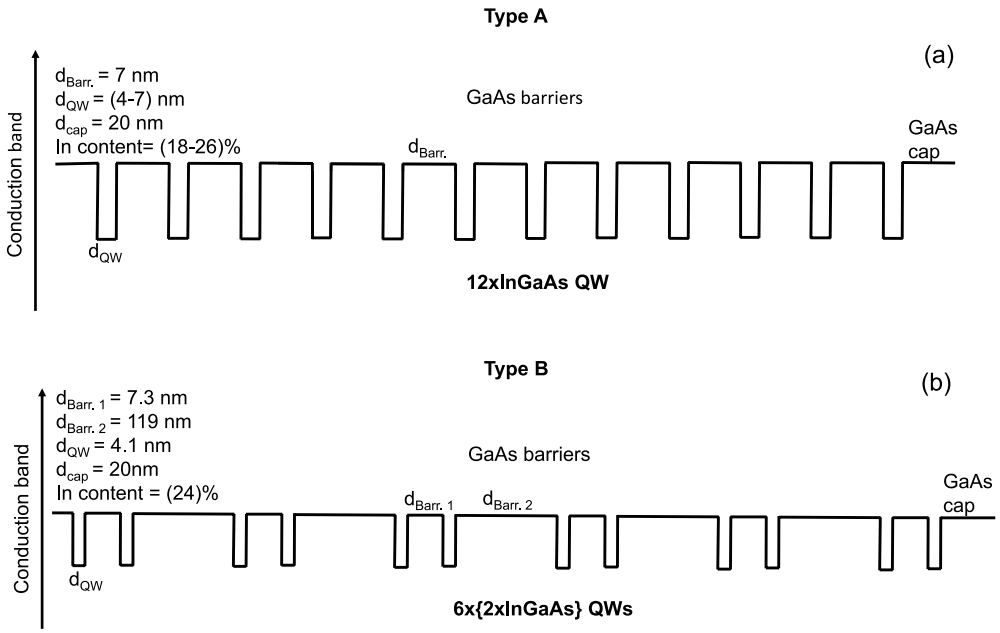


**Fig. 1**. Two types of MQWs structures grown and investigated in this work. (**a**) type A structure comprised of 12 InGaAs QWs with 7 nm thick GaAs barriers, $d_{QW}$ varied from 4.6 nm to 6.6 nm, and the In content from 18.3 % to 25.6 %. (**b**) type B structure in which 6 pairs of InGaAs QWs were grown with alternating GaAs barriers of 7 nm and 119 nm thicknesses, $d_{QW}$ was 4 nm, and the In content 24 %. Thicknesses are not in scale.

expressed as shown in Equation 1. In which $d_{\mathrm{Barr.2}}$ is the thickness of the thick barrier, $d_{\mathrm{Barr.1}}$ is the thin barrier thickness and $d_{\mathrm{QW}}$ is the QW thickness, while $n_{\mathrm{GaAs}}$ and $n_{\mathrm{InGaAs}}$ are the refractive indices of GaAs and InGaAs. For a VECSEL operating at 976 nm with 4 nm QWs and In content of 24% the calculated value of thickness for $d_{\mathrm{Barr.2}}$ is 119 nm.

$$d_{\mathrm{Barr.2}} = \frac{d^{\mathrm{opt}}_{\mathrm{Barr.2}}}{n_{\mathrm{GaAs}}} = \frac{\lambda - 2d_{\mathrm{Barr.1}} \cdot n_{\mathrm{GaAs}} - 4d_{\mathrm{QW}} \cdot n_{\mathrm{InGaAs}}}{2n_{\mathrm{GaAs}}} \tag{1}$$

Moreover, the design with couple of quantum wells makes the gain region more compact, while maintaining the same number of QWs. It has been demonstrated that 7 nm GaAs barrier allows for QW confinement[32], so the thickness of 7 nm for the thin barriers was selected.

To vary the thickness and In content, the strain in the QWs layer was evaluated. The lattice constants of GaAs and $In_xGa_{1-x}As$ are 5.6531 Å and (6.0583-0.405$(1-x)$) Å respectively. Thus, the lattice mismatch between GaAs and InGaAs with 18 % of In is around 1.5 %, using this value and design values for the structure, the excess strain obtained was $f = 0.45$ meaning that the presence of lattice mismatch dislocations, or misfit dislocations can be expected in our samples[33].

All the samples were grown using a solid source MBE system (Veeco GENxplor R & D) equipped with standard cells for metallic In, Ga and unique design of the As source, generating pure arsenic dimers flux.

The samples were grown on quarters of semi-insulating GaAs wafers. Before the growth the substrate was out-gassed at a temperature of 700°C while supplying As overpressure until a clear $2 \times 4$ reconstruction pattern becomes visible.

A 100 nm GaAs buffer layer was then grown at a substrate temperature of 650°C in order to ensure high surface smoothness. The substrate temperature was reduced to 580° C for growth. The temperature was measured via a thermocouple positioned between the heater and the sample, from previous calibrations of the thermocouple by comparison with the temperature measured by BandiT in our system the real substrate temperature during growth is 50° C lower than what indicated by the thermocouple setting. Growth rates of 720 nm/h for GaAs and in the range of (790-940) nm/h for InGaAs were used, during the growth of InGaAs the beam equivalent pressure ratio between As and Ga used was 11, while the ratio between As and In was 12. These values were calibrated in our setup from previous works to obtain high quality InGaAs layers. Finally, a 20 nm GaAs cap layer was grown on top of every sample.

To evaluate the QW thickness, In content and emission energy, X-ray diffraction (XRD) and RTPL spectra have been acquired for every sample. The results obtained are reported in Tables 1.

The samples were named based on the type of structure grown and the In content in the QWs. For the type A structure the In content varied from 18.3 % to 25.6 % and the QW thickness was in the range (6.6-4.2) nm. While for the type B structure an optimized ratio was used, the indium content was 24 % and QW thickness of 4.1 nm.

Indium content in the quantum wells was controlled by changing the ratio between Ga and In flux. The growth rate of the different compounds was measured by monitoring the intensity oscillations of the $in-situ$ reflection high-energy electron diffraction (RHEED). The observation of the RHEED pattern during the growth allows to evaluate the crystalline quality of the layers via reconstruction.

## Characterization

RTPL mappings were carried out using a diode-pumped solid-state laser emitting at the wavelength of 532 nm with the intensity reaching $\approx 5$ kW/cm$^2$ and spot size on the sample $\approx 50$ µm. The detecting system is composed of a 420 nm focal length monochromator, along with thermoelectric cooled InGaAs photodetector. The scanning was performed by a mounting the samples on a motorized xy linear stages (8MT175-100) with a resolution of 0.31 µm. The step size used for the mapping was 0.2 mm.

µ-PL measurements were performed using a Witec 300S microscopy system. A CW laser diode, emitting at 665 nm (Integrated Optics) was used as the excitation source. The laser beam was focused on the sample by a 100x objective lens with a numerical aperture of 0.9. Photoluminescence from the sample was collected by the same objective lens. The PL signal was then directed to a Andor Shamrock spectrometer coupled with a Andor iGus InGaAs camera, which is a thermoelectrically cooled detector.

| Sample | Series | In content (%) | Quantum wells thickness (nm) | Barrier 1 thickness (nm) | Barrier 2 thickness (nm) | Emission energy (eV) | Emission wavelength (nm) |
|---|---|---|---|---|---|---|---|
| Ax0183 | 1 | 18.3±0.2 | 6.6±0.1 | 7.0±0.1 | – | 1.277 | 971 |
| Ax0225 | 1 | 22.5±0.2 | 4.6±0.1 | 7.1±0.1 | – | 1.274 | 973 |
| Ax0232 | 1 | 23.2±0.2 | 5.0±0.1 | 7.1±0.1 | – | 1.263 | 981 |
| Ax0256 | 1 | 25.6±0.2 | 5.0±0.1 | 7.0±0.1 | – | 1.237 | 1002 |
| Ax0241 | 2 | 24.1±0.2 | 4.2±0.1 | 7.3±0.1 | – | 1.276 | 971 |
| Bx0240 | 2 | 24.0±0.2 | 4.1±0.1 | 7.3±0.1 | 119.0±0.1 | 1.275 | 972 |

**Table 1**. Parameters and optical characteristics of the samples used for discussion in this work. In content in the QW, QW thickness and barrier thickness have been evaluated via XRD measurements. The peak energy and wavelength are taken from the photoluminescence spectra. The letter in the sample name refers to the type of structure grown, while the number represents the In content in the QWs.

## Results and discussion

The first series of samples was grown with type A structure, in aims to optimize the In content and thickness of the QWs for an emission of 976 nm.

From the first series of samples four have been selected for discussion. These have been grown with an In content varying from 18 % up to 25.6 % and a QW thickness in between 4.6 nm to 6.6 nm. The barrier thickness was kept at 7 nm. The emission wavelength obtained varied from 971 nm to 1002 nm. In the first four rows of Table 1 the results of the measurements are reported.

To evaluate the homogeneity of the emission from the QWs the intensity correspondent to the maximum of the emission energy was mapped. The maps of the normalized intensity are shown in Fig. 2.

The energy at which the emission intensity was mapped varied from sample to sample, and for each sample the energy at which the maximum was observed in RTPL spectra was selected. Sample Ax0183 in Fig. 2(a) has the lowest In content in the QWs and the thickest QW, 6.6 nm. Sample Ax0225, Fig. 2(b), has the thinnest QWs, 4.6 nm. Ax0232 and Ax0256, Fig. 2(c) and (d) respectively, have the same QW thickness of 5 nm.

These maps clearly show a net where the PL intensity is reduced of 'dark lines'. The map of sample Ax0183 presented in Fig. 2(a), the one with the lowest In content, shows the lowest density of lines of reduced intensity. The majority of these lines are localized next to the edge of the sample. In sample Ax0225 Fig. 2(b) the net of lines covers the entire surface. Comparing Ax0232 Fig. 2(c), and Ax0256 Figure 2(d) that have QWs of the same thickness and only differ in indium content in QWs we can observe that increasing In content leads to the formation of a more densely packed net.

RTPL spectra were measured from different parts of the samples to understand the reason of this reduction of the emission. The results of the measurements performed on sample Ax0256 are shown in Fig. 3. Figure 3(a) shows the map of the entire sample.

Figure 3(b),(c) presents the areas marked on Fig. 3(a) by rectangles from which the spectra were measured. The crosses mark the precise spots, in correspondent colors, the measurements are presented in Fig. 3(d),(e). The investigation of all our samples revealed a similar tendency, the peak position does not change but the intensity reduces.

μ-PL maps were done for investigation with higher resolution. In Fig. 4 the maps of integrated intensity obtained from the samples Ax0183 (a), Ax0232 (b), Ax0256 (c) are reported.

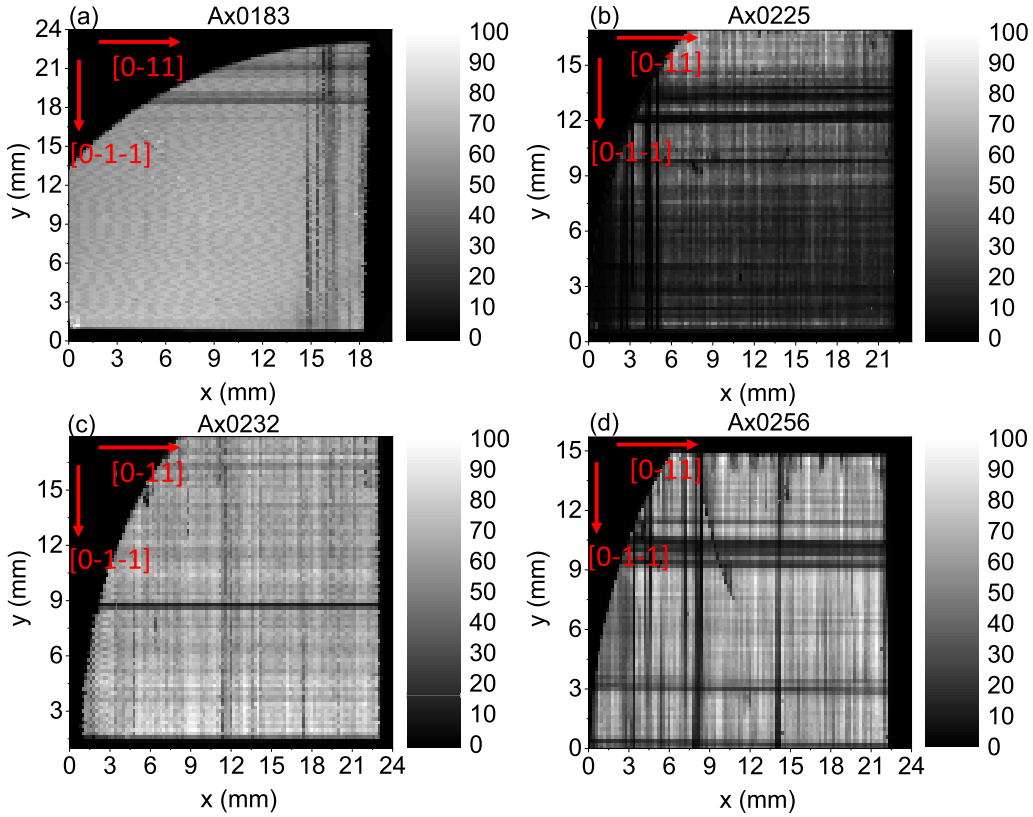


**Fig. 2**. Normalized maps of the first series of samples, the In content in the QWs increases from (**a**) to (**d**). The exact In content, and structural parameters are reported in Table 1. (**a**) Normalized PL map of Ax0183 measured at an energy of 1.279 eV. (**b**) Normalized PL map of Ax0225 measured at an energy of 1.274 eV. (**c**) Normalized PL map of Ax0232 measured at an energy of 1.262 eV. (**d**) Normalized PL map of Ax0256 measured at an energy of 1.237 eV. The dark crack like feature visible in the top left corner of the map is related to the cleaving of the sample.

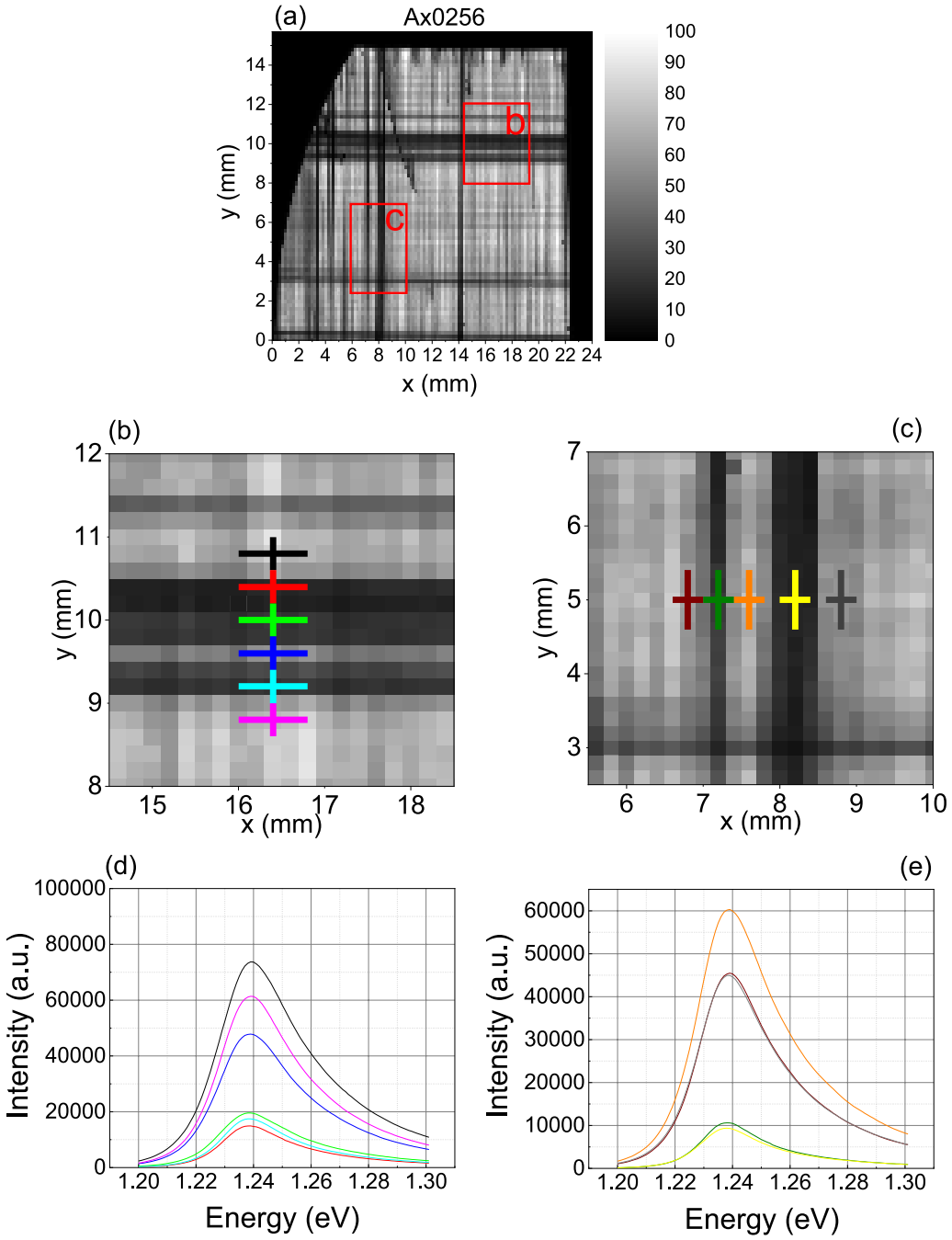


**Fig. 3**. (**a**) RTPL map of sample Ax0256, the two rectangles show the areas that were analyzed in detail, (**b**) the zoomed in $(14.5 \leq x \leq 18.5,\ 8 \leq y \leq 12)$, (**c**) the zoomed in $(5.5 \leq x \leq 10,\ 2.5 \leq y \leq 7)$, (**d**) the spectra were measured along $x = 16.4$, for six different $y$ values. Each spectra was acquired in the spot marked by the cross of the correspondent color, (**e**) the PL spectra measured along $y = 5$ for five different $x$ values. Each spectra was acquired in the spot marked by the cross of the correspondent color.

The images evidence that the lines of reduced emission are present in both cases of thicker QWs and lower In content, and high In content and thinner wells as well as in a combination in between. It is also shown that while in the RTPL maps of Ax0183 lines were not visible (see Fig. 2(a)) in the μ-PL image taken from the middle of the sample, Fig. 4(a), thin lines are present.

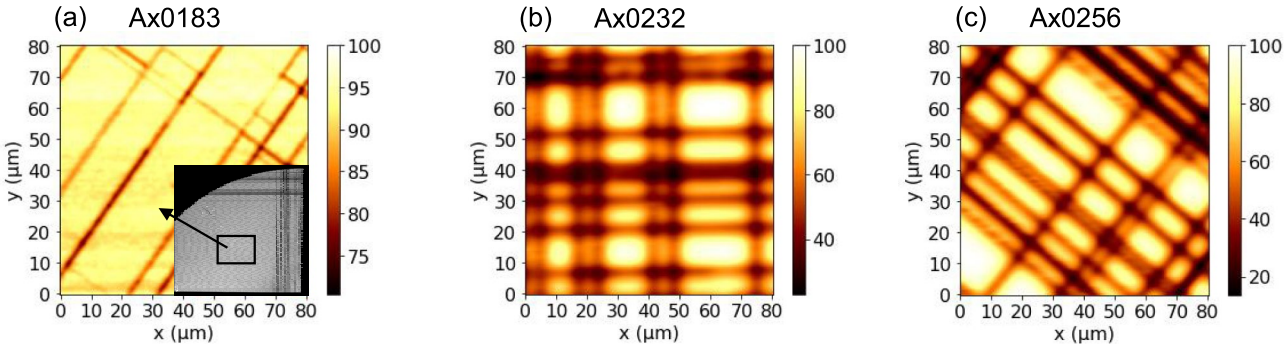


**Fig. 4**. µ-PL measurement performed on sample Ax0183, Ax0232 and Ax0256. The scanned area is $80 \times 80\ \mu m^2$. The crystallographic direction along which the lines appear are [0 −1 −1] and [0 −1 1], as shown in Fig. 2. (**a**) Map relative to Ax0183, the insert shows the RTPL map where the area investigated by µ-PL is highlighted by a rectangle, (**b**) map of sample Ax0232, (**c**) map of sample Ax0256.

Comparing RTPL and µ-PL maps in both Fig. 2 and Fig. 4, with results reported in literature[26,34,35] these reduced intensity lines can be attributed to the presence of dislocations in the QW layers. From the comparison between Ax0232 (Fig. 2(c)) and Ax0256 (Fig. 2(d)) that were grown with the same QW thickness and different In content in the QW, it can be observed that increasing the In content leads to the formation of a more dense net of lattice mismatch dislocations.

The second series of samples was grown to evaluate the effect of the insertion of a thicker barrier between couples of QWs on the homogeneity of the PL intensity. For a more detailed discussion two samples were selected. Ax0241 was grown with barrier thickness of 7.3 nm, while Bx0240 was grown with alternating thin barrier of 7.3 nm and a thick barrier of 119 nm. The data obtained are reported in Table 1, bottom two rows. QW thicknesses were 4.2 nm and 4.1 nm for samples Ax0241 and Bx0240 respectively. The RTPL emission energy measured was 1.276 eV for Ax0241 and 1.275 eV for Bx0240. PL mapping of the samples are shown in Fig. 5. The intensity corresponding to the PL peak of each sample was mapped. In the map of sample Ax0241 Figure 5(a) lines of reduced RTPL emission are visible across the entire sample, matching the observation from the previous set of samples. In the RTPL maps of sample Bx0240 (Fig. 5(c)) lines of reduced PL intensity were not observed.

The µ-PL maps were measured to clarify the results obtained from large area PL maps. µ-PL intensity mapping of samples Ax0241 and Bx0240 are shown in Fig. 5 (b) and (d) respectively. Figure 5(b) demonstrates that lines of reduced emission well match the RTPL map in Fig. 5(a). Figure 5(d) does not show any clear line of reduced intensity, while in Fig. 5(e) shows the homogeneity of the emission across the surface of the sample.

The stress calculations for different structures, compared with the critical stress following the method in Ref[33]., support the presence of misfit dislocations in the A-type samples. When applied to sample Bx240, these calculations show that the stress in this structure also exceeds the critical value, which would typically lead to the formation of dislocations. However, in these calculations, the stress is determined by summing the contributions from each QW and approximating the MQW system as a single QW with higher stress. If we instead assume that the 119 nm barrier in Bx240 is thick enough to reset the stress between pairs of QWs and recalculate the stress for a QW pair, the resulting value is below the critical threshold. This explains the absence of misfit dislocations.

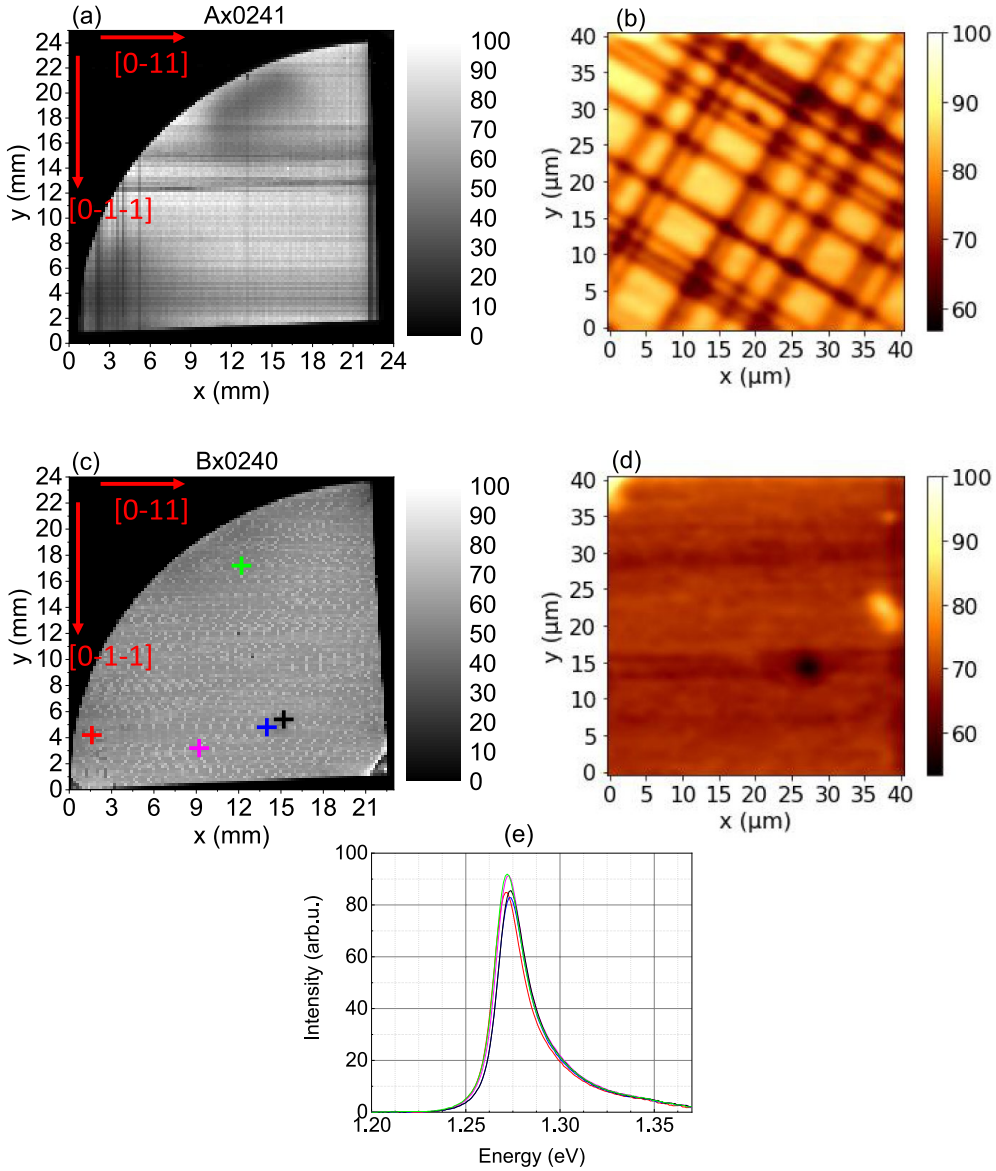


**Fig. 5**. RTPL and µ-PL mappings of the second series of samples. The integrated intensity of the emission has been mapped for the two samples in an area of $40 \times 40\ \mu m^2$. The structural parameters of the samples shown are reported in Table 1. The crystallographic direction along which the lines appear in (**b**) and (**d**) are [0 −1 −1] and [0 −1 1], as shown in (**a**) and (**c**). (**a**) normalized PL map of Ax0241 measured at an energy of 1.276 eV. (**b**) Map of the integrated emission intensity of sample Bx0240 obtained from µ-PL measurements (**c**) normalized PL map of Bx0240 measured at an energy of 1.275 eV. The crosses indicate the position at which spectra were measured (**d**) Map of the integrated emission intensity of sample Bx0240 obtained from µ-PL measurements performed on sample Bx0240. (**e**) PL spectra measured in different points of sample Bx0240, each one corresponds to the cross of the same color.

## Conclusion

The analysis of µ-PL maps revealed the presence of lattice mismatch dislocations in quantum wells structures with thin uniform barrier width and relation between In content, QW thickness and dislocation density. For quantum wells structures, grown with alternating barrier thickness to match QW pairs with the antinodes of standing wave in the gain media of VECSEL, no lattice mismatch dislocations were observed. Our achievements demonstrated benefits of quantum structure design in contrast with previous works[9–11] were uniform barriers were used. We demonstrated that the alternating barrier thickness can be employed in the gain region of a VECSEL aimed at the emission of 976 nm without the need for strain balancing strategies.

## Data availability

The datasets used and/or analysed during the current study available from the corresponding author on reasonable request.

Received: 11 March 2025; Accepted: 22 August 2025
Published online: 25 September 2025

## References

1. Okhotnikov, O. G., Lyytikäinen, J. & Guina, M. Power scalable semiconductor disk lasers for frequency conversion and mode-locking. *Quantum Electron.* **38**, 1083. https://doi.org/10.1070/QE2008v038n12ABEH013965 (2008).
2. Hill, J. et al. Intra-cavity frequency-doubled vecsel system for narrow linewidth rydberg eit spectroscopy. *Opt. Express* **21**, 1–12. https://doi.org/10.48550/arXiv.2206.00096 (2022).
3. Hunziker, L. E. et al. Power-scaling of optically pumped semiconductor lasers. *Int. Soc. for Opt. Photonics* **6451**, 64510A. https://doi.org/10.1117/12.710243 (2007).
4. Fan, L. et al. Multichip vertical-external-cavity surface-emitting lasers: a coherent power scaling scheme. *Opt. Lett.* **31**, 3612–3614. https://doi.org/10.1364/OL.31.003612 (2006).
5. Saarinen, E. J., Härkönen, A., Suomalainen, S. & Okhotnikov, O. G. Power scalable semiconductor disk laser using multiple gain cavity. *Opt. Express* **14**, 12868–12871. https://doi.org/10.1364/OE.14.012868 (2006).
6. Hastie, J. et al. 0.5-W single transverse-mode operation of an 850-nm diode-pumped surface-emitting semiconductor laser. *Photonics Technol. Lett. IEEE* **15**, 894–896. https://doi.org/10.1109/LPT.2003.813446 (2003).
7. Heinen, B. et al. 106 W continuous-wave output power from vertical-external-cavity surface-emitting laser. *Electron. Lett.* **48**, 516–517. https://doi.org/10.1049/el.2012.0531 (2012).
8. Jechow, A., Skoczowsky, D. & Menzel, R. 100 mW high efficient single pass SHG at 488 nm of a single broad area laser diode with external cavity using a PPLN waveguide crystal. *Opt. Express* **15**, 6976–6981. https://doi.org/10.1364/OE.15.006976 (2007).
9. Muszalski, J. et al. VECSELs emitting at 976nm designed for second harmonic generation in the blue wavelength region. *Proc. SPIE - The Int. Soc. for Opt. Eng.* **8702**, 43–49. https://doi.org/10.1117/12.2014757 (2013).
10. Haring, R. et al. High-power passively mode-locked semiconductor lasers. *Quantum Electron. IEEE J.* **38**, 1268–1275. https://doi.org/10.1109/JQE.2002.802111 (2002).
11. Jacquemet, M. et al. Single-frequency cw vertical external cavity surface emitting semiconductor laser at 1003 nm and 501 nm by intracavity frequency doubling. *Appl. Phys. B* **86**, 503–510. https://doi.org/10.1007/s00340-006-2499-0 (2007).
12. Muraki, K., Fukatsu, S., Shiraki, Y. & Ito, R. Surface segregation of in atoms and its influence on the quantized levels in ingaas/gaas quantum wells. *J. Cryst. Growth* **127**, 546–549. https://doi.org/10.1016/0022-0248(93)90680-U (1993).
13. Yee-Rendón, C. M. *et al.* Interdiffusion of Indium in piezoelectric InGaAs-GaAs quantum wells grown by molecular beam epitaxy on (11*n*) substrates. *J. Appl. Phys.* **96**, 3702–3708. https://doi.org/10.1063/1.1783611 (2004).
14. Kaspi, R. & Evans, K. R. Improved compositional abruptness at the InGaAs on GaAs interface by presaturation with In during molecular-beam epitaxy. *Appl. Phys. Lett.* **67**, 819–821. https://doi.org/10.1063/1.115454 (1995).
15. Iba, S. & Ohno, Y. Nanosecond recombination lifetimes and spin relaxation times in (110) InGaAs/AlGaAs quantum wells at room temperature. *Appl. Phys. Express* **17**. https://doi.org/10.35848/1882-0786/ad2907 (2024).
16. Li, B. et al. Temperature dependence of optical property and crystal quality in InGaAs/AlGaAs MQWs grown by MBE. *Opt. Mater.* **162**. https://doi.org/10.1016/j.optmat.2025.116855 (2025).
17. Güniat, L. et al. Nanoscale mapping of light emission in nanospade-based InGaAs quantum wells integrated on Si(100): Implications for dual light-emitting devices. *ACS Appl. Nano Mater.* **5**, 5508–5515. https://doi.org/10.1021/acsanm.2c00507 (2022).
18. Liu, L. *et al.* Low-temperature growth of InGaAs quantum wells using migration-enhanced epitaxy. *Materials* **17**. https://doi.org/10.3390/ma17040845 (2024).
19. Wang, Q. et al. Integrated fabrication of a high strain InGaAs/GaAs quantum well structure under variable temperature and improvement of properties using MOCVD technology. *Opt. Mater. Express* **11**, 2378–2388. https://doi.org/10.1364/OME.431015 (2021).
20. Zou, Y., Esmaielpour, H., Suchet, D., Guillemoles, J.-F. & Goodnick, S. M. The role of nonequilibrium lo phonons, pauli exclusion, and intervalley pathways on the relaxation of hot carriers in InGaAs/InGaAsP multi-quantum-wells. *Sci. Rep.* **13**. 5601. https://doi.org/10.1038/s41598-023-32125-2 (2023).
21. Chan, K., Lightner, M., Patterson, G. & Yu, K. Growth studies of pseudomorphic GaAs/InGaAs/AlGaAs modulation-doped field-effect transistor structures. *Appl. Phys. Lett.* **56**, 2022–2024. https://doi.org/10.1063/1.103005 (1990).
22. Ishikawa, F., Luna, E., Trampert, A. & Ploog, K. H. Critical parameters for the molecular beam epitaxial growth of (Ga, In)(N, As) multiple quantum wells. *J. Appl. Phys.* **89**, https://doi.org/10.1063/1.2372760 (2006).
23. Luna, E., Ishikawa, F., Batista, P. & Trampert, A. Indium distribution at the interfaces of (Ga, In)(N, As)/ GaAs quantum wells. *Appl. Phys. Lett.* **92**. https://doi.org/10.1063/1.2907508 (2008).
24. Fitzgerald, E., Ast, D., Kirchner, P., Pettit, G. & Woodall, J. Structure and recombination in InGaAs/GaAs heterostructures. *J. Appl. Phys.* **63**, 693–703. https://doi.org/10.1063/1.340059 (1988).
25. Jiménez, J. Laser diode reliability: crystal defects and degradation modes. *Comptes Rendus Physique* **4**, 663–673. https://doi.org/10.1016/S1631-0705(03)00097-5 (2003).
26. Ranta, S. et al. Strain compensated 1120nm GaInAs/GaAs vertical external-cavity surface-emitting laser grown by molecular beam epitaxy. *J. Cryst. Growth* **335**, 4–9. https://doi.org/10.1016/j.jcrysgro.2011.08.044 (2011).
27. Houghton, D., Davies, M. & Dion, M. Design criteria for structurally stable, highly strained multiple quantum well devices. *Appl. Phys. Lett.* **64**, 505–507. https://doi.org/10.1063/1.111111 (1994).
28. Hopkins, J.-M. et al. 0.6 W CW GaInNAs vertical external-cavity surface emitting laser operating at 1.32 μm. *Electron. Lett.* **40**, 30–31. https://doi.org/10.1049/el:20040049 (2004).
29. Guina, M., Leinonen, T., Härkönen, A. & Pessa, M. High-power disk lasers based on dilute nitride heterostructures. *New J. Phys.* **11**. https://doi.org/10.1088/1367-2630/11/12/125019 (2009).
30. Korpijärvi, V.-M., Leinonen, T., Puustinen, J., Härkönen, A. & Guina, M. D. 11 W single gain-chip dilute nitride disk laser emitting around 1180 nm. *Opt. Express* **18**, 25633–25641. https://doi.org/10.1364/OE.18.025633 (2010).
31. Korpijärvi, V.-M., Kantola, E. L., Leinonen, T., Isoaho, R. & Guina, M. Monolithic GaInNAsSb/GaAs VECSEL operating at 1550 nm. *IEEE J. Sel. Top. Quantum Electron.* **21**, 480–484. https://doi.org/10.1109/JSTQE.2015.2415200 (2015).
32. Arnaud, G. et al. Photoreflectance and piezophotoreflectance studies of strained-layer $In_xGa_{1-x}As$-GaAs quantum wells. *Phys. Rev. B* **46**, 15290–15301. https://doi.org/10.1103/PhysRevB.46.15290 (1992).
33. Griffin, P. R. et al. Effect of strain relaxation on forward bias dark currents in GaAs/InGaAs multiquantum well p-i-n diodes. *J. Appl. Phys.* **80**, 5815–5820. https://doi.org/10.1063/1.363574 (1996).
34. Ohizumi, Y., Tsuruoka, T. & Ushioda, S. Formation of misfit dislocations in GaAs/InGaAs multiquantum wells observed by photoluminescence microscopy. *J. Appl. Phys.* **92**, 2385–2390. https://doi.org/10.1063/1.1496121 (2002).
35. Wang, J., Steeds, J. W. & Woolf, D. A. The study of misfit dislocations in $In_xGa_{1-x}As$/GaAs strained quantum well structures. *Philos. Mag. A* **65**, 829–839. https://doi.org/10.1080/01418619208205592 (1992).

## Acknowledgements
This article is based upon work from COST Action OPERA – European Network for Innovative and Advanced Epitaxy – CA20116, supported by COST (European Cooperation in Science and Technology, www.cost.eu). This research has also received partial funding from the Research Council of Lithuania (LMTLT), agreement No S-PD-22-7.

## Author contributions
R.B. conceived the project and supervised the research. A.Z. and A.Š. designed and performed the growth of the samples. B.Č., P.W., A.V. and E.D. characterized the optical properties of the structures. S.S. preformed the XRD measurements and modeling. V.D. performed modeling of the samples. R.B., A.Z., M.T. and A.Č. analyzed the results. All of the authors discussed the results and reviewed the original draft. A.V. provided founding.

## Declarations

## Competing interests
The authors declare no competing interests.

## Additional information
**Correspondence** and requests for materials should be addressed to A.Z. or R.B.